applied sciences

MDPI

Article

Optical Breakdown on Clusters of Gas Nanobubbles in Water; Possible Applications in Laser Ophthalmology

Vladimir A. Babenko [1], Andrey A. Sychev [1] and Nikolai F. Bunkin [2,*]

[1] P.N. Lebedev Physical Institute, Russian Academy of Sciences, Leninskiy Prospekt, 53, 119991 Moscow, Russia
[2] Department of Fundamental Sciences, Bauman Moscow State Technical University, ul. Baumanskaya 2-ya, 5/1, 105005 Moscow, Russia
* Correspondence: nbunkin@mail.ru

Abstract: Here we studied the regimes of optical breakdown in water, stimulated by nanosecond and picosecond laser pulses at a wavelength of 1064 nm. A distinctive feature of our theoretical model, confirmed in experiment, is that in our case the optical breakdown develops on heterogeneous centers-clusters of gas nanobubbles. To the best of our knowledge, this is the first study of the role of clusters of gas nanobubbles in the optical breakdown of liquids that are transparent to pump radiation. In the experiment described in this paper, it was found that when initially degassed water is saturated with dissolved air, the breakdown threshold decreases. A theoretical model describing this phenomenon is suggested. This model includes the development of an electron avalanche inside individual nanobubbles, followed by the stimulated optical coalescence of a nanobubble cluster. According to our estimates, this regime occurs at laser radiation intensities of about 10^6–10^7 W/cm^2. It is important that at such low intensities the breakdown flash (the basic endpoint of optical breakdown) does not appear due to the deficit of input laser energy. We provide an experimental proof of the coalescence regime, stimulated by a laser pulse in nanosecond range. The experimental threshold of stimulated coalescence is in good agreement with the theoretical estimates. Since the stimulated optical coalescence mode occurs at very low laser intensities, its excitation does not result in mechanical side effects in eye tissues, i.e., a shock wave should not be excited. Note that shock wave always occurs during optical breakdown, which is traditionally excited at intensities of 10^{12} W/cm^2. In our experiment, the generation of a shock wave at such pump intensities was also observed. Since, according to the estimates given in the article, the volume number density of nanobubble clusters in the intraocular fluid can reach 10^8 cm^{-3}, the excitation of the stimulated optical coalescence mode of nanobubble clusters can be used in ophthalmic surgery, such as laser iridotomy.

Keywords: optical breakdown in water; gas nanobubbles; clusters of gas nanobubbles; stimulated optical coalescence; ophthalmic surgery; laser iridotomy

check for updates

Citation: Babenko, V.A.; Sychev, A.A.; Bunkin, N.F. Optical Breakdown on Clusters of Gas Nanobubbles in Water; Possible Applications in Laser Ophthalmology. *Appl. Sci.* **2023**, *13*, 2183. https://doi.org/10.3390/app13042183

Academic Editor: Takeo Minamikawa

Received: 9 January 2023
Revised: 3 February 2023
Accepted: 5 February 2023
Published: 8 February 2023

Copyright: © 2023 by the authors. Licensee MDPI, Basel, Switzerland. This article is an open access article distributed under the terms and conditions of the Creative Commons Attribution (CC BY) license (https://creativecommons.org/licenses/by/4.0/).

1. Introduction

The interaction of laser radiation with medium in a condensed state has recently been studied; see, for example, recent works [1–4]. Local thermal and thermo-elastic effects are shown in this work. These effects can be used in surgical practice. In this connection, laser technologies are widely used in ophthalmic surgery. The optically transparent structures of the eye, i.e., cornea, lens and vitreous body, make the delivery of laser pulse energy in the visible and near infrared spectral range much easier than in other tissues, thereby allowing surgical operations to be performed without destroying the areas, which are sensitive to light, e.g., the retina. Radiation with different wavelengths, pulse durations and intensities interacts with the tissues of the eye in different ways. For example, continuous-wave green light is used for the local thermal pinpoint coagulation of the retina, while nanosecond pulses in the ultraviolet region of the spectrum are used for high-precision superficial tissue

ablation, for example, to change the shape of the corneal surface; see reviews [5,6] for more details.

The first type of pulsed laser that was successfully used in ophthalmology was the YAG:Nd^{3+} laser, emitting at wavelength of $\lambda = 1064$ nm. The cornea, lens and vitreous are transparent at this wavelength. Nanosecond pulses at this wavelength are widely used in ophthalmologic operations; the energies of these pulses typically lie in the range of 0.3–10 mJ [7].

In the case where YAG:Nd^{3+} laser pulses are tightly focused inside the eye up to a size of several microns, the pulses of nanosecond duration produce an intensity of about 10^{11}–10^{12} W/cm^2 at the focal area of the lens. Under these conditions, a phenomenon called "optical breakdown" occurs. This effect is characterized by a sufficiently bright flash of light, which is visible to the naked eye. The reason for the appearance of such a flash consists in rapidly increasing electron density in the liquid bulk. When this density exceeds approximately 10^{20} cm^{-3}, a plasma flash in the focal area of the lens is formed [6]. At such intensities, a macroscopic cavitation bubble appears in water; this process is accompanied by the generation of a shock wave and tissue destruction [8]. The cavitation bubble makes several pulsations and eventually collapses, which leads to the generation of another shock wave [6]. All these effects are often referred to as the "photodegradation" of tissue.

The radii of cavitation bubbles belong to the range of 1–2 mm, and at typical pulse energies of the YAG:Nd^{3+} laser the amplitudes of shock waves at a distance of 1 mm from the focus reach up to 100–500 bar [9]. These harmful side effects limit the use of nanosecond laser pulses in ophthalmology. When lasers with picosecond pulses became available, their mechanical side effects appeared less, but were still too great for many ophthalmic applications. This limits the use of nanosecond and picosecond pulses in clinical ophthalmology [10].

Recently, femtosecond laser pulses have been used in ophthalmology. The reason for that is the rather low energy of the femtosecond laser pulse, which leads to a sharp decrease in mechanical side effects. For example, if we are dealing with 300 fs pulses with an energy of 0.75 μJ, the generated cavitation bubbles have a radius of only 45 μm, which is almost two orders of magnitude less than for nanosecond pulses with energies, which amounts to several mJ, see Ref. [11]. In addition, for femtosecond pulses, the pressure waves arising during optical breakdown are much weaker, and reach about 1–5 bar at a distance of 1 mm from the breakdown area [12]. Finally, the thermal effects of femtosecond pulses in living tissues are negligible [6].

Note that in all works on optical breakdown in pure water, the breakdown threshold was determined by the onset of a breakdown flash. For the appearance of a visible flash at a wavelength of $\lambda = 1.064$ μm for the nanosecond range, the radiation (threshold) intensity should be $I \sim 10^{11}$ W/cm^2, whereas for the picosecond range the threshold intensity $I \sim 10^{12}$ W/cm^2, and for pulses with a duration of 10–100 fs the threshold intensity $I \sim 10^{13}$ W/cm^2; see the review [13].

In this work, we study a special mechanism of optical breakdown at a wavelength of $\lambda = 1.064$ μm, where breakdown centers are clusters of nanobubbles filled with dissolved gas (atmospheric air). As shown in our previous works [14,15], nanobubbles and clusters of nanobubbles always exist in water, which is saturated with dissolved gas and contains an ionic additive. It seems obvious that such clusters also exist in the intraocular fluid, since this fluid is very close in its properties (basically, the content of dissolved ions) to physiological saline solution, which contains an ionic component. Therefore, the excitation of optical breakdown on clusters of nanobubbles, in our opinion, looks promising for laser applications in ophthalmology. Indeed, the best treatment for pupillary-block glaucoma is to create a tiny hole in the iris (known as an iridotomy). The iridotomy allows the flow of fluid to the front of the eye to be restored, bypassing the location of the blockade. A laser beam is used to burn a small hole in the iris, which releases pressure in the eye. The purpose of this procedure is precisely to reduce the pressure inside the eye; that is, to reduce the likelihood of glaucoma. We hypothesize that this operation can be carried out due

to breakdown inside nanobubble clusters, and the threshold intensity for such a specific breakdown turns out to be significantly lower than the threshold intensities indicated in review [13].

As will be shown in Appendix A, optical breakdown on clusters of nanobubbles that serve as breakdown centers occurs in two stages. The first stage is the coalescence (merging together) of the clusters, which is accompanied by the formation of micron-sized gas bubbles. If the laser pulse has not ended at the moment of formation of such a bubble, and the energy of the laser pulse is still large enough, then laser-induced plasma is generated inside the bubble, and a light flash of breakdown occurs due to the bremsstrahlung effect, which is the basic end point of optical breakdown in liquids. In the case of breakdown on the nanobubble clusters, the cluster coalescence is generated the earlier and the higher the laser pulse intensity (see Appendix A), and at sufficiently high intensities an optical breakdown flash always takes place, which leads to undesirable side effects associated with the mechanical damage of the eye tissues. The purpose of this work is to find the experimental conditions under which laser-stimulated coalescence occurs, but the energy of the laser pulse is still low, and visible breakdown flash is not excited.

Now, it is necessary to explain how gas nanobubbles and their clusters arise in a liquid far from boiling point. Recently, a large number of publications, devoted to the study of the nanobubbles in the bulk of a liquid, have appeared; see, for example, [16–25]. The effects, associated with the clustering of gas nanobubbles, have also been recently studied; see [26,27]; the study of the properties of nanobubbles and their clusters seems to be a hot topic. When studying such tiny bubbles in a liquid, the question of their stability arose; see, for example, review [28]. One of the mechanisms that can provide the stability of nanobubbles is the compensation of surface tension forces by the electrostatic repulsion of anions, adsorbed on the nanobubble surface; see [29]. Therefore, such nanobubbles were termed bubstons (bubble, stabilized by ions). The work [29] theoretically predicted that individual bubstons could coagulate with one another in water and aqueous salt solutions to form clusters of bubstons; the theoretical aspects of bubston coagulation with the formation of the cluster phase are presented in [30].

The existence of separate bubstons was proved in experimental works [31,32], and the existence of the bubston-cluster phase was confirmed in [33–35]. In these works, bubstons and bubston clusters were studied by using the technique of dynamic light scattering, as well as in experiments on the study of the angular dependences of the scattering matrix elements by using polarization scatterometry. In addition to the techniques based on light scattering, there also exists an alternative technique based on the excitation of optical breakdown. This technique is applicable because bubstons and bubston clusters are the centers of laser breakdown, which was recognized in a recent review on optical breakdown and plasma formation in water, see Ref. [36].

Recently, we have shown [37–39] that the technique of optical breakdown of liquids transparent to laser radiation can be used to study certain characteristics of individual bubstons. In particular, it turned out that the optical breakdown threshold in water containing the bubston phase is close by order of magnitude to the excitation threshold of various nonlinear optical processes, for example, stimulated Raman and hyper-Raman scattering.

Note that in Refs. [37–39] the optical breakdown was studied under the assumption that the breakdown centers are separate bubstons. At the same time, no experiments have been carried out in which the specific features of optical breakdown on the bubston clusters as breakdown centers were examined. The aim of this work is to study the peculiarities of optical breakdown on bubston clusters, induced by nanosecond and picosecond laser pulses at wavelength $\lambda = 1064$ nm. As is known [40], the absorption coefficient in water at this wavelength at room temperature is 0.12–0.13 cm^{-1}; i.e., obviously, the heating, associated with the absorption, can be neglected.

Various regimes of optical breakdown in water at $\lambda = 1064$ nm for pulses of different durations are described in detail in Ref. [13]. As noted in this work (see also numerous articles cited in this review), the breakdown mechanisms of water, free of solid impurities,

are multiphoton absorption, as well as cascade ionization. It was shown in [13] that the breakdown due to cascade ionization occurs in two steps: (i) cascade initiation through the creation of seed electrons and (ii) cascade buildup to the substantially high density of free electrons. Cascade initiation requires at least one or more free electrons to be present in the focal volume at the beginning of the laser pulse. These 'seed' electrons in an impure liquid are most likely to come from the ionized impurities in the focal area prior to the laser pulse. In a pure liquid (free of external solid or liquid particles), "seed" electrons can be produced only due to the ionization of liquid molecules. Since we consider water samples, which were preliminary purified from foreign particles, the initial density of "impurity" electrons in the bulk of water must be equal to zero; that is, seed electrons in our case can appear only as a result of the multiphoton ionization of molecules in the liquid bulk, which requires the very high energy of a laser pulse. Indeed, as shown in review [13], the optical breakdown threshold due to the multiphoton ionization of water molecules at a wavelength of 1064 nm for the pulses with a duration of 10 ns (this wavelength and pulse-width were used in our experiments, see below) is about 10^{11} W/cm^2. As will be shown below, cluster coalescence is induced at the intensities of about 10^6–10^7 W/cm^2, i.e., at much lower intensities. Therefore, it is straightforward to assume that in our case the impurity electrons can be localized inside gas nanobubbles, on the inner surface of which anions are adsorbed, see [30,31]; i.e., the source of seed electrons is the presence of negatively charged particles at the nanobubble (bubston) interface.

In Appendix A, we present a theoretical model of optical breakdown (in CGSE units) that describes on a semi-quantitative level the specifics of optical breakdown on the bubston clusters—the centers of breakdown. We also present experimental evidence that the optical breakdown threshold on bubston clusters is controlled by the content of dissolved gas. These results obviously do not fit into the model of the multiphoton ionization of water molecules in the bulk of water but can be interpreted precisely within the framework of the approach that bubstons and bubston clusters serve as centers of optical breakdown in water free of foreign impurities. The study presented below, as far as we know, is the first work where the role of bubston clusters in the optical breakdown of water was analyzed.

2. Materials and Methods

2.1. Photos of Bubston Clusters

In Figure 1, we exhibit a pattern of the track of a continuous wave (CW) low-intensity laser radiation with a wavelength of λ = 532 nm, scattered at 90 degrees in deionized water. In addition, the liquid samples were filtered by forcing the liquid through a highly hydrophilic polymer track membrane (purchased from Sartorius, Germany), which is made of high-quality polycarbonate. The capillary structure of the pores of these membranes is uniform; the pores are also evenly distributed over the membrane surface, allowing the best retention of particles. The pore size was 300 nm; thus, individual bubstons with a radius of 100 nm pass through the membrane, but bubston clusters larger than a micron in size are filtered out by such a membrane. Note that immediately after filtering, the scattered radiation track is absolutely homogeneous, so we do not present this pattern here. After filtration, the liquid sample was settled for 24 h in a cell in a dust-free room; i.e., an access of solid impurity particles to the sample was excluded. In Figure 1, we present a snapshot of the track after such settling.

The radiation was focused with a lens of long focal length F = 100 mm. In this case, the beam radius in the lens waist is approximately 20 microns, and the waist length is about 2 mm; this is exactly the length of the white bar in Figure 1. Note that the track of scattered radiation contains local bright dots, whose size should exceed the wavelength λ = 532 nm; i.e., these are the so-called Mie scatterers, see, for example, monograph [41]. Since fine filtration does not remove individual bubstons from the liquid, but removes bubston clusters, the appearance of large-scale scatterers can only be associated with the coagulation of bubstons (the formation of clusters) in the process of settling.

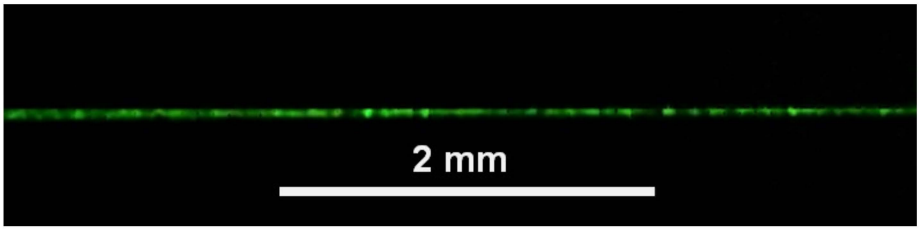


Figure 1. Scattering pattern of continuous low-intensity laser radiation with a wavelength λ = 532 nm in the lens beam waist F = 100 mm in a cell with water, containing the clusters of nanobubbles. The bright flashes are seen against a weak uniform background. These flashes are related to scattering centers, whose size exceeds the wavelength.

Bubston clusters can also be observed with a conventional optical microscope (see Figure 2); the photograph was taken in the dark field of a microscope. A 100 μm layer of water was uniformly illuminated with CW laser light at wavelength λ = 532 nm. Bright inclusions with vague boundaries are clearly seen against a dark background. It is obviously due to the fact that the optical density of these inclusions is less than the optical density of water. Indeed, according to the results of [14,30], the refractive index of bubston clusters in the visible range is n_b = 1.26, while for water the refractive index is n = 1.33. An important feature of bubston clusters is the absence of a clear interphase boundary between the cluster and the surrounding liquid, in contrast to micron-sized gas bubbles. Indeed, as was shown in [32], bubston clusters are fractal objects; therefore, there is no geometric concept of an interface for such objects. This is why the diffraction patterns of visible light on the bubston clusters cannot be obtained.

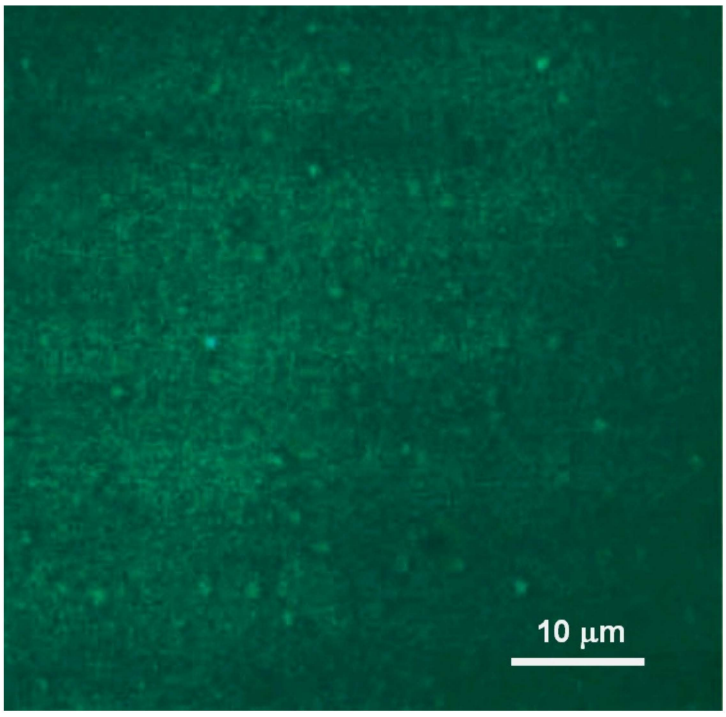


Figure 2. Bubston clusters; photograph in the dark field of an optical microscope.

2.2. Study of Optical Breakdown with Nanosecond Laser Pulses of Low Intensity

Below, we describe an experiment the results of which can be interpreted as direct evidence of the stimulated optical coalescence of bubston clusters. The schematic diagram of the setup for this experiment is shown in Figure 3. We used a pulse-periodic laser with wavelength λ = 1064 nm (1), operating in the Q-switching mode; the pulse duration was τ = 10 ns. The laser operated on the basic transverse mode with a divergence of 3 mrad

and a repetition rate of 2 Hz. A part of laser radiation (2) was converted into the second harmonic (λ = 532 nm) using the DKDP crystal (not shown in this Figure). The laser pulse was directed with a set of lenses and a telescope (3) and entered the cell (4) with the liquid under study. The liquid sample was Milli-Q water. A luminescence screen (a sheet of white paper, (5)) was placed behind the cell in the far-field zone. A characteristic pattern, consisting of a set of bright and dark rings, occurring due to diffraction of second harmonic radiation on a micron-sized gas bubble (see below), was projected onto this screen. The diffracted beam was directed with a lens system (6) to the input of the Hamamatsu S1226-5BQ avalanche photodiode (7), which receives signals in the visible and near UV ranges. The avalanche photodiode was connected to a Tektronix MDO34 oscilloscope (bandwidth 1 GHz), which was used to control the duration of the second-harmonic pulse, resulting from the diffraction of incident light by a gas-vapor bubble. Summarizing, here we applied the known pump-probe technique to study the dynamics of laser breakdown, see, e.g., the review [13].

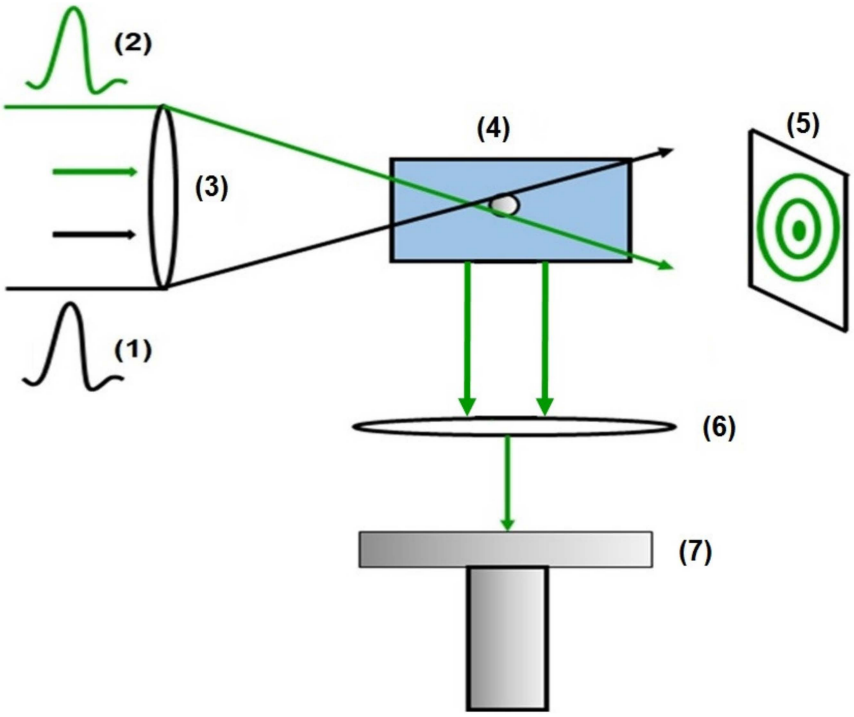


Figure 3. Schematic diagram of the experimental setup for observing the effect of stimulated optical coalescence. (1)—laser pulse at a wavelength λ = 1064 nm; (2)—laser pulse at a wavelength of 532 nm; (3)—lens system; (4)—cell with liquid; (5)—screen for observing the instantaneous diffraction pattern; (6)—lens system; (7) Hamamatsu S1226-5BQ avalanche photodiode.

2.3. Study of Optical Breakdown with Picosecond High Intensity Laser Pulses

The schematic diagram for investigating optical breakdown in the field of high intensity picosecond laser pulses is shown in Figure 4.

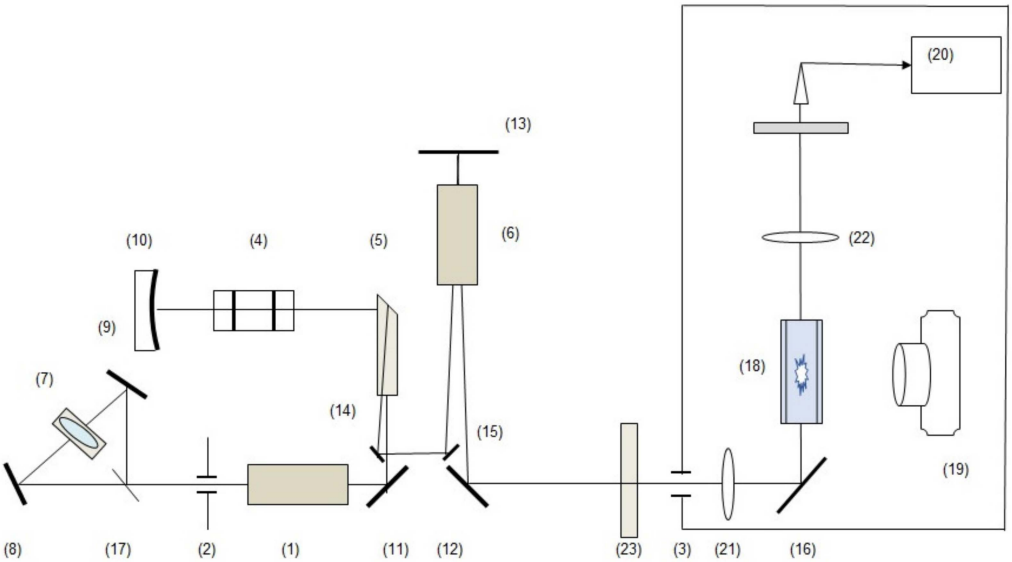


Figure 4. Schematic of the experimental setup. (1)—active element of YAG:Nd3+; (2), (3)—diaphragms (∅ = 2.5 mm); (4) electro-optical modulator (DKDP crystal); (5)—polarizing prism; (6) YAG:Nd3+ amplifier; (7)—passive shutter in the Sagnac interferometer; (8)–(16)—mirrors (reflection coefficient R = 1.0); (17)—semitransparent mirror (reflection coefficient R = 0.5); (18)—cell with test water; (19)—camera; (20)—spectrometer; (21), (22)—focusing lenses; (23)—notch-filter that transmits only radiation at wavelength λ = 1064 nm.

A single laser pulse with a wavelength (λ = 1064 nm) and a duration of 20 ps was separated from a train of ultrashort pulses (the laser setup is described in detail in [42]). Stable generation was achieved due to the temporal coincidence of saturation of the gain of the active medium and transmission of the passive shutter (the so-called "second generation threshold"). The time profile of the laser pulse was controlled by an electro-optical converter with a time resolution of 6 ps (not shown in Figure 4). Figure 5 shows a typical snapshot of a single laser pulse with a duration of τ = 20 ps at a wavelength of λ = 1064 nm, reflected from two surfaces of a beam-splitting glass plate installed at an angle of 45° to the optical axis and diverting part of the laser pulse to the input of a high-speed streak camera.

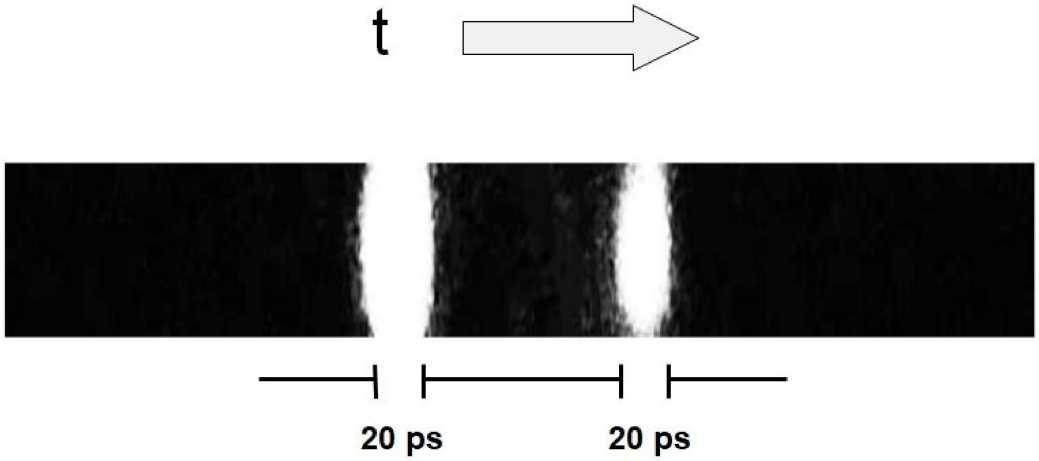


Figure 5. Time scans of a laser pulse recorded with a high-speed streak camera. Two signals correspond to the reflection from two surfaces of glass plate, which divert part of the laser pulse to the input of the streak camera. The time delay between scans corresponds to a double pass through the glass plate.

3. Results

3.1. Experiment with Low-Intensity Nanosecond Laser Pulses

The idea of the experiment with low-intensity nanosecond laser pulses, the schematic setup of which is exhibited in Figure 3, is as follows. According to our model (see Appendix A), the optical breakdown in individual bubstons is caused by the collisions of electrons, driven by the electric field of the light wave, with water molecules of the bubston liquid walls. If a bubston cluster appears in the focal area of a laser beam, an electron avalanche develops inside each bubston. Obviously, the collisions of electrons with the liquid walls of the bubston cluster are elastic; that is, the electrons efficiently accumulate energy and heat up, see Ref. [43] for more details. In this case, a rapid expansion of individual bubstons within the cluster occurs, which ends with the coalescence (merging together) of the cluster and the formation of a macroscopic vapor–gas bubble of micron size (the bubble size is about the size of the bubston cluster itself). We called this process stimulated optical coalescence.

As shown in Appendix A, if the laser pulse has not ended by the time of the formation of the macroscopic bubble, the electrons continue to oscillate due to the electric field of the light wave, but in this case the electrons will collide with heavy particles (fragments of the liquid walls of the bubston cluster), and during such collisions the electrons will transfer their momentum to heavy particles and experience deceleration, which will be accompanied by the emission of bremsstrahlung quanta, see Appendix A.

The further evolution of a macroscopic bubble includes the growth of a vapor–gas bubble up to millimeter size, pulsations and collapse, which is accompanied by the generation of a shock wave. It is obvious that such an optical breakdown mode is not applicable in ophthalmic applications, since undesirable side effects inevitably arise in this case. At the same time, at low energies of laser pulses, it is possible to choose such a regime when the entire pulse energy will be spent solely to the stimulation of the optical coalescence of a bubston cluster. According to the estimates presented in Appendix A, the intensity of laser radiation at the wavelength $\lambda = 1064$ nm, which is sufficient to complete the coalescence process, is about 10^7 W/cm^2. For that intensity, the coalescence time for a bubston cluster with a size of 1 micron (such a cluster includes several hundred individual bubstons) is about $t_{coal} = 10^{-10}$ s; i.e., for nanosecond pulses, coalescence finishes at the front of the laser pulse. Obviously, for higher intensities, stimulated optical coalescence can occur much earlier, see Appendix A. The micron-sized bubble formed as a result of coalescence is unstable and collapses according to diffusion kinetics. Indeed, it was theoretically shown in [44] that the lifetime of unsteady bubbles is proportional to the square of their radius; in accordance with the estimates given in this work, the lifetime of a micron non-stabilized micron bubble at room temperature (that is, far from the boiling point) is of the order of 10 msec.

In the experiment, the schematic setup of which is illustrated in Figure 3, we attempted first to demonstrate the fact that the coalescence stage does exist in the optical breakdown, and second to estimate the coalescence threshold. To observe the coalescence, it was very important to make sure that the directions of beams at wavelengths of 1064 and 532 nm strictly coincide with one another along the entire path of both beams. To satisfy this condition, the position of the DKDP crystal was aligned in such a way that a characteristic dark area should appear in the center of the green spot, projected on a luminescence screen (see Figure 6). This dark area appears in the case of a complete coincidence of both beams for the following reason. Radiation at the second harmonic is stronger deflected by the focusing lens; therefore, its focus is localized in front of the focus of the beam at the first harmonic along the propagation of both beams. Here, we should take into account that the radiation at wavelength $\lambda = 1064$ nm is slightly absorbed in water (the absorbance is 0.14 cm^{-1}), while absorption in water at wavelength $\lambda = 532$ nm can be neglected. Since $dn/dT < 0$, where n is the refractive index of water (see Ref. [45]), we are dealing with a weak negative thermal lens, arising along the propagation of both beams. This thermal lens efficiently deflects the second harmonic rays away from the focus area. It is clear that the

dark area in the center of the green spot can appear only in cases where the directions of rays of the first and second harmonics exactly coincide. The fact that darkening is associated namely with the weak thermal lens was verified by placing a spectral filter, opaque for IR radiation but transparent for the visible region, in front of the cell with liquid; in this case, darkening disappeared.

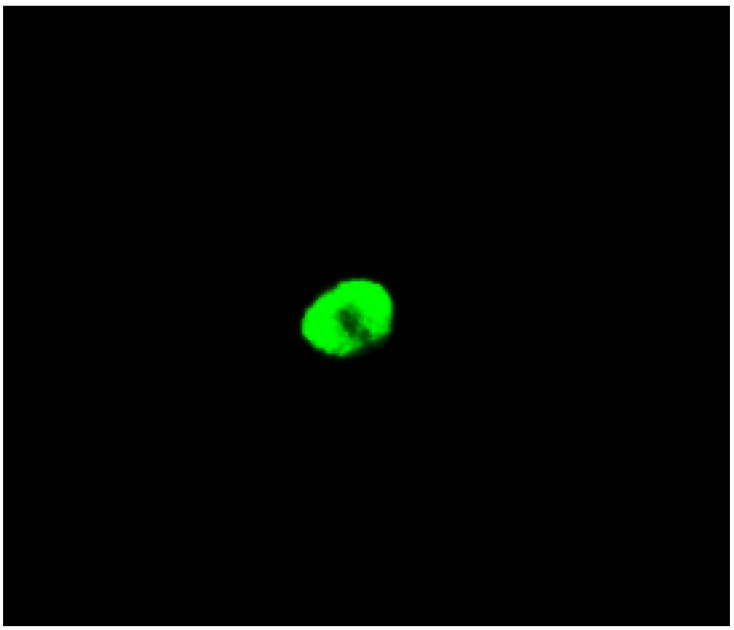


Figure 6. Light spot of the second harmonic. The dark area in the spot center is caused by the thermal lens.

Under the irradiation of water with laser pulses with a certain intensity at the wavelength of 1064 nm, instantaneous diffraction patterns appeared on the luminescence screen. We used a mask cutting the central radiation maxima for the first and second harmonics (Figure 7) to prevent direct light incidence on the CCD array of the camera, which was used for snap-shooting the patterns on the screen. The size of the object, resulting in the diffraction, was estimated by the period of diffraction rings; this size was about 1–5 μm. Thus, it was found that the laser shooting of water results in the formation of objects of such sizes. These objects instantly disappear if water is under normal conditions. If water was maintained at a temperature slightly less than the boiling point, we observed the formation of vapor bubbles under the same experimental conditions; i.e., liquid boiled before reaching the boiling point. Thus, we claim that the objects at which the second harmonic beam is diffracted are vapor–gas bubbles. In this experiment, it is important that the coalescence regime arose at intensities of the order of 10^6–10^7 W·cm^{-2}, which is close to the estimate in Appendix A. A macroscopic vapor–gas bubble (which is a negative lens with respect to laser radiation) is formed at the laser pulse front. To initiate an optical breakdown inside such a bubble, laser radiation should be introduced into such a bubble, which obviously requires a higher laser pulse energy compared to the energy applied to generate this bubble. It is clear that, at the energy of threshold of stimulated optical coalescence, the laser beam cannot penetrate into the bubble, and no optical breakdown spark (plasma flash) occurs.

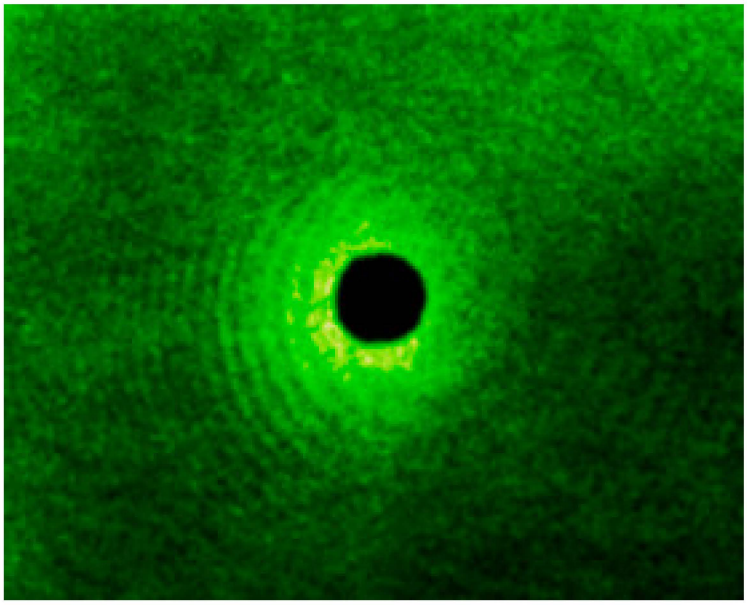


Figure 7. Diffraction pattern for the second harmonic; the mask cuts direct radiation.

In Figure 8, we exhibit an oscillogram of the second harmonic pulse at sensor (7) in Figure 3. The duration of this pulse is 8.5 ns, which approximately coincides with the duration of the pump pulse τ = 10 ns, which was to be expected. In this experiment, we did not have the opportunity to measure the lifetime of the gas bubble after the completion of the stimulated optical coalescence. It is clear, however, that the spherical bubbles formed during coalescence disappear almost instantly after completing the laser pulse, since there is no stabilization mechanism for these bubbles, see Ref. [44] for more details.

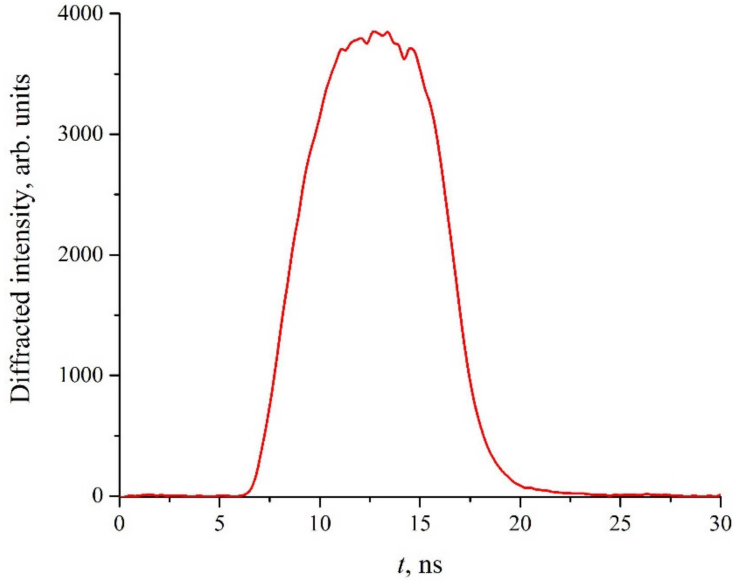


Figure 8. Temporal profile of the intensity of the second-harmonic pulse, which diffracted on a gas-vapor bubble, arisen as a result of forced optical coalescence.

Summing up, we can claim that at weak laser intensities the optical breakdown, which is characterized by a bright flash, does not occur because of low energy in the pulse, whereas micron-sized spheres are formed due to the stimulated optical coalescence of the bubston cluster.

3.2. Experiment with High-Intensity Picosecond Laser Pulses

In the experiments with high-intensity picosecond laser pulses, we studied the threshold of the optical breakdown of water I_{thr} induced by a 20 ps laser pulse (λ = 1064 nm). In this experiment, the onset of optical breakdown was fixed by the appearance of a bright light flash (the basic endpoint of optical breakdown); that is, the stage of optical coalescence should be completed by the time the flash appears. Typical photographs of breakdown flashes at the intensities $I \approx 0.9$ TW/cm^2 and 1.2 TW/cm^2 are shown in Figure 9a,b. The plasma flash was recorded at an angle of 90° to an optical axis (this photodetector is not shown in Figure 4).

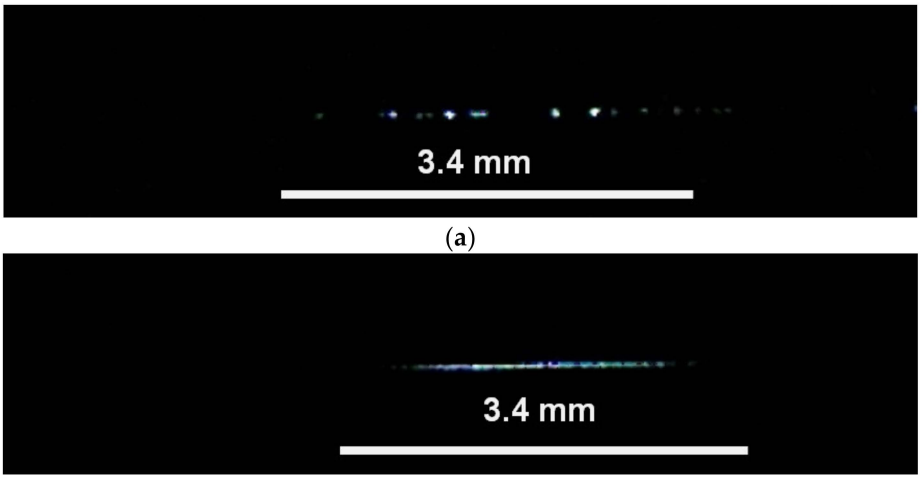


Figure 9. Flash patterns at the focus of a long-focus lens (F = 100 mm) in water saturated with bubston clusters, induced by laser pulse (τ = 20 ps, λ = 1064 nm). Panel (**a**) is related to intensity at the breakdown threshold, $I \approx 0.9$ TW/cm^2; panel (**b**) is related to intensity $I \approx 1.2$ TW/cm^2.

As shown in Appendix A, at the laser pulse intensity of about 10^7 W/cm^2, stimulated optical coalescence occurs at times of the order of 10^{-10} s. However, with increasing intensity, all dynamic processes leading to the stimulated optical coalescence of the bubston cluster are significantly accelerated. Therefore, at intensities of the order of 10^{12} W/cm^2, the stimulated optical coalescence should be completed within times less than 20 picoseconds, and in this case a plasma flash of optical breakdown occurs. In experiments with high-intensity picosecond pulses, the threshold intensities I_{thr} for the occurrence of optical breakdown flash in degassed water and water, saturated with dissolved gas, were studied. Degassing was carried out by the prolonged boiling of the liquid under vacuum; the degassing technique is described in detail in a recent paper [46]. A highly sensitive receiver (photoelectron multiplier FEU-79, LLC Zapadpribor, Moscow, Russia, not shown in Figure 4) made it possible to fix the plasma emission of optical breakdown Lum_{BR} at $I \approx I_{thr}$. In Figure 10, we exhibit the dependence of Lum_{BR} vs. the laser pump intensity in the focal area of a short-focus lens (F = 20 mm) for degassed Milli-Q water. The threshold value of the breakdown intensity for such water was I_{thr} = 3.0 TW/cm^2, and this value remained unchanged in time providing that the liquid sample was kept in a hermetically sealed cell (i.e., without access of atmospheric air).

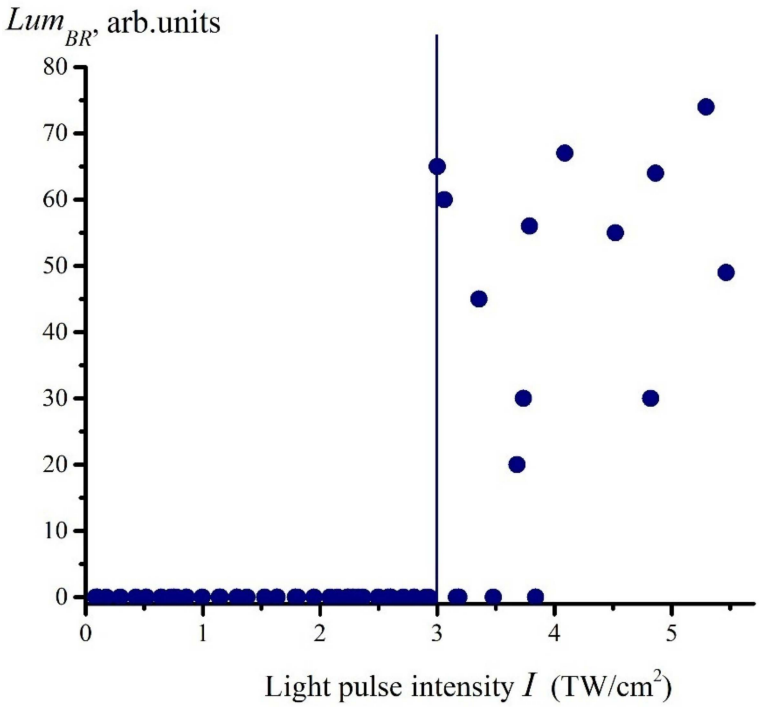


Figure 10. Dependence of the breakdown flash intensity Lum_{BR} vs. the pump intensity I at the focal area (F = 20 mm) for degassed Milli-Q water.

It turned out that the contact of degassed water with atmospheric air leads to a decrease in the optical breakdown threshold from I_{thr} = 3.0 TW/cm^2 to I_{thr} = 0.85 TW/cm^2 within the time T = 12 h of settling the degassed sample in open atmosphere. Note that this value significantly exceeds the threshold intensity for stimulated optical coalescence, which is about 10^7 W/cm^2.

4. Discussion

As follows from the data of review [13], for laser pulses at the wavelength λ = 1064 nm with a duration τ = 60 ps and a spot diameter in the beam waist d = 31 μm the breakdown threshold intensity I_{thr} = 0.14 TW/cm^2. Furthermore, it was found in [47] that for the pulses with a duration of τ = 30 ps and spot diameter d = 19.5 μm the breakdown threshold is I_{thr} = 0.37 TW/cm^2. The indicated diameters of d approximately correspond to the spot diameter in our experiments, i.e., d_0 = 40 μm. The value of the threshold intensity measured in [47] agrees in order of magnitude with the value I_{thr} = 0.85 TW/cm^2, which was measured in our experiments in water saturated with dissolved gas, i.e., consisting of the phase of bubston clusters.

It should be noted that the experimental works considered in review [13] do not report on the samples of degassed water. At the same time, as was obtained in our experiments, the experimental breakdown threshold for degassed samples is I_{thr} = 3 TW/cm^2, which noticeably exceeds the breakdown threshold for the same water saturated with dissolved gas, i.e., having the bubston clusters. Thus, our results essentially refine the data presented in review [13]: in the case of the optical breakdown of water saturated with dissolved gas, the presence of bubston clusters, which serve as local breakdown centers, should be taken into account.

The pattern of optical breakdown on bubston clusters near the threshold corresponds to a set of discrete plasma flashes; each flash corresponds to the breakdown inside a separate cluster, see Figure 9a. Assuming that there are four bright flashes (i.e., four clusters) in the volume of the caustic (a cylinder with a radius of 20 μm and a length of 3.4 cm), we obtain an estimate for the volume number density of clusters $n_{cl} \approx 10^6$ cm^{-3}, which is consistent

with the estimate in [35], obtained on the basis of polarization scatterometry; in accordance with this work, $n_{cl} = 0.5 \times 10^6$ cm^{-3}.

It should be noted that, after the completion of the picosecond laser pulse, the glow of the breakdown plasma is controlled by radiative processes, the duration of which can exceed the duration of the laser pulse, see [13,47]. All this leads to the initial breakdown pattern, consisting of individual plasma flashes (Figure 9a), turning into a "smeared" breakdown pattern shown in Figure 9b. The blurring process is due to the plasma expansion and the effect of moving the breakdown site, see Ref. [13].

The model of moving breakdown assumes that breakdown occurs independently at multiple sites along the beam path; i.e., we are dealing with multiple breakdown. The multiple breakdown occurs whenever the threshold is reached at each breakdown site. In our case, it is straightforward to assume that these breakdown sites are the bubston clusters localized along the caustic. Since the optical breakdown, accompanied by a plasma flash, leads to the generation of a shock wave, the breakdown region expands with the speed of the shock wave, and we can estimate this speed from indirect data. The expansion of the breakdown region due to the movement of the plasma front results in the formation of a new plasma pattern, elongated in the direction of the laser beam from the original breakdown site. The resultant plasma pattern along the caustic looks more uniform due to the merging together of the local breakdown sites, see Figure 9b. Following [13], for the maximum length of the plasma area we have an empirical formula $z_{\max} = z_R(\beta - 1)1/2$, where $\beta = I/I_{thr}$, z_R is the caustic length, $\lambda = 1064$ nm. In our case $z_R = 3.4$ mm.

Thus, at $\beta \approx 1$, there will be no blurring effect of local breakdown sites (apparently, this situation is illustrated in Figure 9a), while in the case of $\beta \geq 1$, each plasma point will experience a slight blurring; that is, the breakdown pattern will take the shape exhibited in Figure 9b; in this case $(\beta - 1)^{1/2} = (1.2/0.85 - 1)^{1/2} = 0.64$; that is, the value of $z_{\max}$ will be slightly less than the length of the caustic z_R. Let us now estimate the velocity u of the plasma front at which the pattern of the plasma flash becomes uniform along the caustic. Let us assume that the volume number density of clusters is equal to about 10^6 cm^{-3}; that is, the average distance between clusters is $l \approx 100$ μm. In addition, we assume that for the spatial homogeneity of the flash, the plasma front must cover the distance $l/2 \approx 50$ μm during the plasma flash. Taking $\tau_{pl} = 1.6$ ns for the plasma flash duration (this value was taken from study [47] for plasma glow during the optical breakdown of water excited by an 80 ps pulse at wavelength $\lambda = 1064$ nm), we obtain the estimate $u = l/(2\tau_{pl}) = 31$ km/s; i.e., here we are dealing with a shock wave of very high intensity. Therefore, optical breakdown at laser pulse intensities in the range $I \sim 10^{12}$ W/cm^2 is obviously not applicable in ophthalmology, since the shock wave should inevitably lead to undesirable side effects. At the same time, in the case of breakdown on bubston clusters, the first stage of breakdown is stimulated optical coalescence, which requires quite moderate intensities (of the order of 10^7 W/cm^2) to occur. If the intensity of laser radiation is fixed at this level, then a plasma flash will not occur; that is, it will be possible to avoid the appearance of a shock wave.

According to the results of this work, the volume number density of bubston clusters in doubly distilled water saturated with dissolved gas $n_{cl} \approx 10^6$ cm^{-3}. As shown in [32], the volume number density of bubston clusters can be estimated using the empirical formula $n_{cl} = \kappa/\sigma_{sca}$, where κ is the extinction coefficient of radiation at a wavelength of 532 nm in an aqueous salt solution; σ_{sca} is the scattering cross section of radiation at this wavelength on a separate bubston cluster. Note that at this wavelength the absorption of light in water is absent; that is, extinction is due only to scattering by particles exceeding the wavelength in size. In [32], the extinction coefficient was measured in a dust-free aqueous solution of NaCl in the concentration range $10^{-3} < C < 3$ M. As shown in this work, for ion concentrations $C < 1.5$ M, the values of the dependence of extinction coefficient κ, measured in the experiment on laser light scattering vs. C, can be approximated by the empirical formula $\kappa = \alpha(C - C_0)^{1/2}$, where α is a dimensional constant and C_0 is the lower limit of ion content at which bubston clusters are formed; this quantity was not determined by us. Assuming that the scattering cross section σ_{sca} does not depend on the content of ions,

we obtain that an increase in the ion concentration by a factor of 100 should lead to an increase in the volume number density n_{cl} of bubston clusters by approximately a factor of 10. In a physiological solution of NaCl (this solution is apparently close by its properties to intraocular fluid), the content of ions is $C = 0.14$ M, while for doubly distilled water we have an estimate of $C = 10^{-6}$ M. Thus, the volume number density of bubston clusters n_{cl} in physiological saline solution should increase by about 300 times compared to doubly distilled water, i.e., $n_{cl} \approx 10^8$ cm^{-3}. Therefore, bubston clusters are likely to be centers of optical breakdown in intraocular fluid.

5. Conclusions

The main result of this work is as follows. It has been established that in the case of optical breakdown on bubston clusters as heterogeneous breakdown centers, the breakdown develops in two stages. At the first stage, the coalescence (merging) of the cluster occurs, followed by the formation of a macroscopic gas bubble. In this case, the size of such a bubble cannot exceed the size of the cluster itself; i.e., this size is about 1 micron. If the laser pulse has not yet finished to the moment of the coalescence completion, the secondary electrons, resulting from the ionization of the nanobubble liquid walls, keep oscillating subject to the optical wave, which leads to collisions of these electrons with heavy particles. These particles are "fragments" of the liquid walls of the cluster, and the collisions of electrons with these particles are obviously not elastic; that is, the electrons in these collisions lose their energy, which is accompanied by bremsstrahlung. In this case, the resulting bubble continues to expand and can reach sizes of the order of 1–2 mm, which is accompanied by a powerful shock wave, see [9,13].

If the intensity of laser pulses does not exceed the threshold value for the cluster coalescence, which belongs to the range of 10^6–10^7 W/cm^2, then the entire pulse energy is completely spent on the coalescence process; i.e., no flash of optical breakdown is observed, and the size of the resulting bubble does not exceed 1 micron. The lifetime of micron bubbles is limited by the rate of the diffusion of gas molecules from this bubble into the bulk of liquid. Thus, in the range of laser radiation intensities of 10^6–10^7 W/cm^2 at wavelength $\lambda = 1064$ nm, the effect of a laser pulse is reduced only to the generation of a micron-sized gas bubble. It is clear that the bubble formed as a result of coalescence does not have time to heat up; that is, the temperature of such a bubble should be close to room temperature, and the shock wave, obviously, appears neither at the end of cluster coalescence (arising of the bubble), nor at the diffusion collapse of the bubble, since the diffusion is a very slow process. For room temperature, in accordance with the results of [44], we have an estimate of $\tau \approx 10^{-2}$ s for the lifetime of such a micron-sized bubble.

It should be expected that when performing ophthalmic operations using laser radiation at intensities of 10^6–10^7 W/cm^2, mechanical side effects caused by the excitation of a shock wave during the generation and collapse of millimeter-sized bubbles will not manifest themselves; that is, the excitation of the stimulated optical coalescence of nanobubble clusters can be used in ophthalmologic surgery, for example, in laser iridotomy.

Author Contributions: Conceptualization, N.F.B.; investigation, V.A.B., A.A.S.; writing—original draft preparation, N.F.B.; supervision, N.F.B. All authors have read and agreed to the published version of the manuscript.

Funding: This research received no external funding.

Institutional Review Board Statement: This study did not require ethical approval.

Informed Consent Statement: Not applicable.

Data Availability Statement: The data presented in this study are available on request from the corresponding author.

Conflicts of Interest: The authors declare no conflict of interest.

Appendix A

If a gas nanobubble (bubston) exists in the focal area of a laser beam, an electron avalanche can develop inside this nanobubble. The process of an avalanche developing depends on the relationship between the nanobubble (bubston) radius R_0 and the average free path of electrons l_{em} with respect to their collisions with gas molecules inside the bubston. The length $l_{em} = 1/(n\sigma_{em})$ where σ_{em} is the transport cross-section of electrons scattering on the molecules, $\sigma_{em} = (2 - 4) \times 10^{-16}$ cm^{-2}, $n = p/T$ is the density of the molecules and p is the pressure on the bubble surface (hereinafter T is expressed in energy units). For the bubston, the surface tension pressure $2\alpha/R_0$ (α is the surface tension coefficient) is compensated by the electrostatic expansive (negative) pressure ${Q_0}^2/(8\pi\varepsilon {R_0}^4) = 2\pi\sigma^2/\varepsilon$, caused by the adsorption of ions on the inner bubble surface (σ is the surface charge density and ε is the dielectric constant) [29]. This is why, for bubstons, pressure p is always equal to hydrostatic pressure p_0, which is close (under laboratory conditions) to the external (atmospheric) pressure at the liquid interface. Accordingly, under normal conditions $n = n_L = 2.7 \times 10^{19}$ cm^{-3} (the Loschmidt number). Thus, the length l_{em} is about 10^{-4} cm and always exceeds the bubston radius $R_0 = 100$ nm, see [30]; in this work, the radii of individual bubstons were found in the experiments with dynamic light scattering and phase microscopy.

The opposite inequality $l_{em} < R_0$ can take place under normal conditions only for unstable bubbles, which can exist under non-stationary conditions. For such bubbles, the pressure $2\alpha/R_0$ is not compensated, and therefore $p = p_0 + 2\alpha/R_0 > p_0$. As is known, such bubbles are not stable; see, for example, [44]. However, for water and some other liquids under normal conditions, the difference between p and p_0 is valid only for $R_0 < 10^{-4}$ cm. This is why for $R_0 > 10^{-4}$ cm we have $p = p_0$, $n = n_L$ and, accordingly, $l_{em} = 10^{-4}$ cm $< R_0$. It will be shown below that such bubbles can be generated at the final stage of the stimulated optic coalescence (SOC) of bubston clusters. The SOC effect is the basis for the suggested model of optical breakdown in liquids. Qualitatively, this model is as follows. The development of an electron avalanche inside bubstons, which compose a cluster, leads to the rise of pressure inside individual bubstons, resulting in their expansion, and to the merging into a "large" bubble. This is the SOC effect.

As we have already mentioned, bubston clusters consist of stable gas nanobubbles (bubstons) with radii $R_0 << l_{em}$. Initial free electrons (i.e., the electrons that always exist inside the nanobubble) arise due to the adsorption of anions at the interface of inner liquid walls, see [31]. Despite the fact that $R_0 << l_{em}$, an electron avalanche can develop inside such a bubston. Electron density should grow due to the increase in the energy of electron chaotic motion, stimulated by collisions with the bubble wall at the frequency $\nu_{ew} = \langle v_e \rangle / R_0$ and due to the ionization of wall molecules (here $\langle v_e \rangle$ is the mean arithmetical velocity of electrons) rather than due to their collisions with gas molecules (as is the case when $R_0 >> l_{em}$). The ionization frequency is $\nu_i = \dot{Y}_e/\Delta$, where Δ is the ionization energy and $\dot{Y}_e$ is the average rate of increasing energy Y_e of electron chaotic motion. For the electromagnetic wave frequency with $\omega > \nu_{ew}$ we obtain, using the approach presented in [43]

$$\dot{Y}_e = 2\nu_{ew} Y_{vib} = \nu_{ew} \frac{e^2 E_0^2}{2m\omega^2} = \nu_{ew} \frac{I}{c n_{ecr}}. \quad \text{(A1)}$$

Here, Y_{vib} is the average kinetic energy of the vibrational motion of electrons in the optical wave with amplitude E_0 and frequency ω, $n_{ecr} = m\omega^2/(4\pi e^2)$ is the critical electron density and $I = c{E_0}^2/(8\pi)$ is the wave intensity. In our particular case (the wavelength $\lambda = 1064$ nm), we obtain $n_{ecr} \approx 3 \times 10^{19}$ cm^{-3}.

The only way to decrease the number of electrons in the process of avalanche development is their adhering to the liquid bubble wall. The frequency of such a process is $(\langle v_e \rangle / R_0) w_{a,e}$, where $w_{a,e}$ is the probability of electron adhesion. If ionization frequency $\nu_i > (\langle v_e \rangle / R_0) w_{a,e}$, the electron avalanche should start; in accordance with our model, this is the condition of the breakdown threshold. The avalanche development rate depends on the pump intensity I; for large I, an essential ionization can occur at the stage of the inertial

retention of the nanobubble, i.e., before its radius substantially grows. The increase in the number of electrons N_e inside a bubston due to the avalanche development is determined by the equation

$$dN_e/dt \;=\; N_e/\theta(I), \tag{A2}$$

where the avalanche time constant $\theta = \theta(I)$ obeys the condition

$$\theta^{-1}(I) \;=\; \frac{\langle v_e\rangle w_{a,e}}{R_0}\left(\frac{I}{I_0}-1\right). \tag{A3}$$

Here, the parameter $I_0 = cn_{e\mathrm{cr}}\Delta w_{a,e}$. During the avalanche development, i.e., when an electron loses its energy to ionization, the electron distribution over the energies $f(Y_e)$ may be considered to be stationary within the range $0 < Y_e < \Delta$, since the electrons with energy $Y_e > \Delta$ quickly disappear due to the ionization of molecules on the liquid wall. The function $f(Y_e)$ can be determined approximately on the basis of the following simple assumptions. The probability $f(Y_e)dY_e$ is proportional to the duration of electron location in the energy interval $(Y_e, Y_e + dY_e)$, i.e., is proportional to $dY_e/\dot{Y}_e$, where $\dot{Y}_e$ means "genuine" (not the average, by contrast to Equation (A1)) energy growth rate; i.e., $\dot{Y}_e$ is proportional to the "genuine" electron velocity $v_e \;=\; \sqrt{2Y_e/m}$. Thus, we obtain $f(Y_e) \;=\; c/\sqrt{Y_e}$, where c is a dimensional constant, and after normalizing to the energy interval $(0, \Delta)$ we arrive at $f(Y_e) \;=\; Y_e^{-1/2}/2\sqrt{\Delta}$. The mean energy $\langle Y_e\rangle$, which will be called the electron avalanche temperature T_e, is equal to

$$\langle Y_e\rangle \;=\; T_e \;=\; \int_0^{\Delta} Y_e f(Y_e)dY_e \;=\; \Delta/3,$$

and the mean arithmetical velocity is $\langle v_e\rangle \;=\; \sqrt{3T_e/2m}$. Surface ionization energy Δ can be much less than the ionization energy of an individual molecule of liquid. In the following estimates we will assume $\Delta \approx 6$ eV (see, e.g., [48,49]), and, correspondingly, $T_e = 2$ eV, $\langle v_e\rangle = 7 \times 10^7$ cm/s, and the frequency of collisions $\nu_{ew} = 7 \times 10^{12}$ s^{-1}. Electron avalanche development inside a nanobubble with the radius $R_0 << l_{em}$ has one more peculiarity as compared with the case $R_0 >> l_{em}$. This follows from the fact that here the molecules of the liquid wall, rather than gas molecules, are being ionized, and therefore the avalanche electrons form a "pure" electron gas (but not a quasi-neutral plasma), which is confined by the sphere of radius R_0. The surface of this sphere obviously acquires a uniformly distributed positive charge $Q = e \times N_e$. The Coulomb repulsion in the electron gas affects both the rate of the electron avalanche and the dynamics of bubston expansion during the SOC process. It is clear that, at the stage of inertial retention (see below), avalanche development is governed by Equations (A2) and (A3) only for small average electron density inside the bubble $\langle n_e\rangle = N_e/(4\pi {R_0}^3/3)$, i.e., when the free path length associated with electron-electron collisions is larger than R_0. When the average density $\langle n_e\rangle$ increases, the frequency of electron collisions with the wall must drop ("peripheral" electrons shield the wall from the collisions with "central" electrons) and consequently avalanche development ceases (electron-electron collisions do not contribute to the absorption of light). It follows from here that there should exist a maximum value of the average electron density, which should depend on the bubston radius, i.e., $\langle n_{e\max}\rangle = \langle n_{e\max}\rangle\,(R_0)$. This value is to be determined.

Electron gas inside a bubston must have non-uniform distribution owing to the Coulomb interaction, i.e., its density $n_e = n_e(r)$, where r is the distance from the bubston center. The problem of determining $n_e(r)$, and the corresponding electrical potential $\varphi(r)$ distribution is the classical Debye problem, which can be solved under the condition

$n_e << (T_e/e^2)^3 = 2.7 \times 10^{21}$ cm^{-3} (see, for instance, [50]). Assuming the validity of the Boltzmann distribution for the electron density and considering this distribution,

$$n_e(r) \;=\; n_e(0)\exp(3e\varphi/2T_e) \approx n_e(0)(1+3e\varphi/2T_e)$$

in the area $0 < r < R_0$, we find that the Poisson equation $\nabla^2\varphi = -4\pi\rho = 4\pi e n_e(r)$ can be rewritten as

$$\nabla^2\varphi - \varphi/a_e^2 \;=\; 4\pi e n_e(0), \tag{A4}$$

where

$$a_e \;=\; \sqrt{T_e/6\pi e^2 n_e(0)}$$

is the Debye radius for electrons. Solving this equation, we should impose the following boundary conditions: the first condition $\varphi(0) = 0$, and the second condition

$$4\pi\int_0^{R_0} r^2 n_e(r)dr \;=\; N_e. \tag{A5}$$

It is easy to show that the solution $\varphi(r)$ satisfying the first condition is the following

$$\varphi(r) \;=\; \frac{T_e}{e}\left(\frac{\sinh r/a_e}{r/a_e} - 1\right), (0 \le r \le R_0). \tag{A6}$$

For the distribution $n_e(r)$ we obtain

$$n_e(r) \;=\; n_e(0)\frac{\sinh r/a_e}{r/a_e}. \tag{A7}$$

In accordance with Equation (A5), N_e has the following form

$$N_e \;=\; \frac{2T_e R_0}{3e^2}\frac{x\cosh x - \sinh x}{x}, \tag{A8}$$

where $x = R_0/a_e$. For the large values of N_e, i.e., when $x > 1$, this equation can be presented as

$$x \;=\; \ln\frac{3N_e e^2}{T_e R_0} + \ln\frac{1}{1-1/x}. \tag{A9}$$

According to Equations (A4), (A7) and (A8), $n_e(0)$ and $n_e(R_0)$are equal to

$$n_e(0) \;=\; \frac{T_e x^2}{6\pi e^2 R_0^2}, n_e(R_0) \;=\; \frac{N_e x}{4\pi R_0^3}. \tag{A10}$$

It is clear that $n_e(0)$ depends on N_e only logarithmically, and $n_e(R_0)= \langle n_e\rangle \times (x/3)$, where $\langle n_e\rangle = N_e/(4\pi {R_0}^3/3)$ is the mean density of electrons. While N_e grows, electron gas is being compressed in the spherical layer of thickness $a_e = R_0/x$ close to the bubble surface. In the case of a large value of N_e, electrons are "stuck" in this layer and stop colliding with the wall. This happens when the electron free-path length in this layer $l_{ee}= 1/(\sigma_{ee} n_e(R_0))$ (here $\sigma_{ee} \;=\; (9/16)\pi e^4/T_e^2$, see [51]) is equal to

$$l_{ee} \;=\; \frac{16}{9}\frac{T_e^2}{\pi e^4 n_e(R_0)} \;=\; \frac{16}{3}\frac{T_e^2}{\pi e^4\langle n_e\rangle x},$$

and becomes less than the layer thickness $a_e = R_0/x$, so we obtain for the mean electron density

$$\langle n_e\rangle \;=\; \langle n_e\rangle_{\max} \;=\; \frac{16}{3}\frac{T_e^2}{\pi e^4 R_0}. \tag{A11}$$

This value is to be considered as the maximum (limiting) quantity, which restricts the electron avalanche development in the nanobubble. For T_e = 2 eV we obtain $\langle n_e \rangle_{\max} = 3 \times 10^{19}$ cm^{-3}, and the total maximum value

$$N_{e\max} = \langle n_e \rangle_{\max} \frac{4\pi}{3} R_0^3 = 2 \times 10^5.$$

It should be noted that the value N_e relates only to the partial ionization of the monomolecular surface layer of the bubble liquid wall. For the total ionization of the layer, we have the estimate $4\pi {R_0}^2 \times {n_l}^{2/3} \approx 1.2 \times 10^6$, where n_l is the density of liquid molecules, $n_l = 3.3 \times 10^{22}$ cm^{-3}. Let us find now the distribution of $n_e(r)$ for $N_{e\max} = 2 \times 10^5$. In accordance with Equation (A9), $x = x_{\max} \approx 8.4$, and therefore $n_e(0) \approx 5 \times 10^7$ cm^{-3}, $n_e(R_0) \approx 1.33 \times 10^{20}$ cm^{-3}, $a_e = 6 \times 10^{-7}$ cm. Below, we will use the results (A6)–(A11) when examining the expansion of the bubstons during the SOC process.

Let us now estimate the value of light wave intensity I, for which the mean electron density $\langle n_e \rangle = \langle n_e \rangle_{\max}$, resulting from the electron avalanche, accumulates inside the bubston prior to its expanding; we will term this stage as the process of inertial retention. As will be shown later, in this case the light intensity coincides with the threshold for the SOC effect, and therefore we denote it by I_{thr}. We denote the inertial retention duration as t_0. Assuming that, while expanding, the nanobubble keeps its spherical form, dependent on the initial radius R_0, let us introduce the quantitative parameter ζ of the retention extent as

$$\zeta R_0 = \int_0^{t_0} u(t) dt, \tag{A12}$$

where $u(t) = dR/dt$, and $\zeta < 1$; that is, the radius of the bubston within the time t_0 grows less than twice. It means that the retention time t_0 is a function of ζ. The specific value of ζ is, of course, dependent on the required accuracy of the calculations. This question, however, is facilitated by a weak dependence of t_0 on ζ. In order to evaluate $t_0 = t_0(\zeta)$ it is necessary to know the rate $u(t)$. The bubston expansion develops due to quickly increasing electron pressure $p_e = p_e(t)$, which is caused by the exponential growth of electron number N_e (according to Equation (A2)). Hence, under the inertial retention conditions, the mean electron density

$$\langle n_e \rangle = N_e \left(\frac{4\pi}{3} R_0^3 \right)^{-1} = \langle n_e \rangle_{\max} \exp(t/\theta - L_{\max}), \tag{A13}$$

where $L_{\max} = \ln[N_{e\max}/N_e(0)] = \ln(1.4 \times 10^5) = 11.8$ (it is assumed here that $N_e(0) = 1$). Providing that $p >> p_0$, where p_0 is the hydrostatic pressure, the velocity $u(t)$ obeys the equation (see [52])

$$R\dot{u} + \frac{3}{2} u^2 = p_e/\rho. \tag{A14}$$

Here, ρ is the density of liquid. At $t = 0$ the radius $R = R_0$, and the velocity $u(t)$ can be deduced from the linearized equation (A14), i.e., when the second term is neglected, and $R = R_0$. Thus, for the velocity $u(t)$ we obtain

$$u(t) = \frac{1}{\rho R_0} \int_0^t p_e dt. \tag{A15}$$

The pressure p_e is the sum of kinetic electron gas pressure $p_{gas} = ne(R_0)T_e$ and the pressure $p_{Coul} = E^2(R_0)/8\pi$, caused by the Coulomb repulsion of electrons. Here, $E(r) = -d\varphi/dr$ is the electric field strength inside a bubston. According to Equation (A6), we have

$$E(r) = \frac{T_e a_e}{e^2 r^2} [\sinh(r/a_e) - (r/a_e)\cosh(r/a_e)], \tag{A16}$$

and, using Equation (A9) at $x > 1$, we find for p_{Coul}

$$p_{Coul} = \frac{\pi}{3}\left(\frac{x-1}{x}\right)^2 (eR_0\langle n_e\rangle)^2 = \left(\frac{x-1}{x}\right)^2 2\pi\sigma^2,$$

where $\sigma = eN_e/4\pi{R_0}^2$ is the surface charge density. Thus, the total pressure at the bubston surface $p_e = p_{gas} + p_{Coul}$ can be presented as

$$p_e = \langle n_e\rangle \frac{T_e x}{3}\left(1 + \pi\left[\frac{x-1}{x}\right]^2 \frac{e^2 R_0^2 \langle n_e\rangle}{T_e}\right). \quad (A17)$$

The expansion rate $u(t)$ can be found on the basis of Equations (A13), (A15) and (A17). Here, we should take into account that, according to Equation (A13), the pressure plays an essential role only at the time of the avalanche development $t \sim \theta \times L_{\max}$, while $\langle n_e\rangle \sim \langle n_e\rangle_{\max}$, $x = x_{\max}$. This is why, when integrating in (A15), the quantity x (which depends on N_e only logarithmically) can be regarded as a constant, equal to $x_{\max} \approx 8.4$. Thus, we arrive at

$$u(t) = u_0^2 \frac{\theta}{R_0}[\exp(t/\theta - L_{\max}) + \mu \exp 2(t/\theta - L_{\max})], \quad (A18)$$

where

$$u_0 = \sqrt{(x_{\max}/3)\langle n_e\rangle_{\max} T_e/\rho} \approx 7.8 \times 10^3 \quad (A19)$$

and parameter

$$\mu = \frac{8}{3x_{\max}}\left(\frac{x_{\max}-1}{x_{\max}}\right)^2 \frac{T_e R_0}{e^2} \approx 31 \quad (A20)$$

This parameter stands for the contribution of the Coulomb repulsion of electrons in the process of bubston expansion. Substituting (A18) in (A12) and taking into account that, in accordance with the definition of I_{thr} (see above), $t_0 = \theta(I_{thr}) \times L_{\max}$, we obtain for the dependence $t_0(\zeta)$

$$t_0 = \left(\frac{\zeta}{1+\mu/2}\right)^{1/2} \frac{R_0}{u_0} L_{\max}. \quad (A21)$$

The threshold intensity I_{thr} is determined from Equation (A3) after substituting either $\theta(I_{thr}) = t_0/L_{\max}$ at laser pulse duration $\tau > t_0$, or $\theta(I_{thr}) = \tau/L_{\max}$ at $\tau < t_0$. Thus, we have for the threshold intensity

$$I_{thr} = I_0\left[1 + \frac{L_{\max}}{(\langle v_e\rangle/R_0)w_{a,e}} \times \max\left(\frac{1}{t_0}, \frac{1}{\tau}\right)\right]. \quad (A22)$$

In the case of $w_{a,e} << 10^{-3}/\zeta^{1/2}$, the second term in (A22) essentially exceeds unity, and we obtain

$$I_{thr} = c\Delta n_{e\mathrm{cr}} \frac{L_{\max}}{\langle v_e\rangle/R_0} \times \max\left(\frac{1}{t_0}, \frac{1}{\tau}\right). \quad (A23)$$

The case of $\tau > t_0$ is more interesting. In this case, according to (A22), we have

$$I_{thr} = c\Delta n_{e\mathrm{cr}}(u_0/\langle v_e\rangle)\left(\frac{1+\mu/2}{\zeta}\right)^{1/2}. \quad (A24)$$

It is evident from Equations (A22)–(A24) that the threshold intensity I_{thr} does not depend on characteristics of molecular gas inside bubstons and is completely controlled by parameters of liquid, such as the energy of surface ionization Δ, the probability of electron adhesion $w_{a,e}$, liquid density ρ and radius R_0 of bubstons. In the case of $\tau > t_0$, dependence on R_0 is realized only due to the fact that $u_0 \sim (R_0)^{-1/2}$ (see Equation (A19)), and due to the dependence $\mu(R_0)$, see (A20). It is clear that I_{thr} increases slowly while R_0 drops. As shown in [29], R_0 depends on the dielectric constant of the liquid, its temperature, surface

tension coefficient, the adsorption energy of the surface ions of the dissolved electrolyte and its concentration. The characteristics of dissolved gas manifest themselves in the optical breakdown process only as a result of the ability of gas to be dissolved in liquid. These remarkable peculiarities allow us to speak about the optical breakdown of liquid but not about the breakdown of gas.

Let us numerically estimate the time t_0 and threshold intensity I_{thr}. They depend on the extent (the measure) of inertial retention ζ. Assuming $\zeta = 0.1$, and bearing in mind that $w_{a,e} << 10^{-3}$ and $L_{\max} = 11.8$, $\mu = 31$, we obtain $t_0 \approx 0.1 \times 10^{-9}$ s, and the threshold intensity for $\tau > t_0$, $\lambda = 1$ μm ($n_{e\mathrm{cr}} = 3 \times 10^{19}$ cm^{-3}) and $\Delta = 6$ eV due to the fact (A24) is equal to $I_{thr} = 9.6 \times 10^6$ W/cm^2. Note that this theoretical estimate is 5–6 orders of magnitude less than the experimentally measured values for the appearance of an optical breakdown flash in water, which is shot with nanosecond YAG:Nd^{3+} laser pulses, see review [13].

Let us demonstrate that the threshold intensity I_{thr}, determined by Equations (A23) and (A24), is sufficient not only for the accumulation of maximum (limiting) mean electron density $\langle n_e \rangle = \langle n_e \rangle_{\max}(R_0)$ inside a bubston within the time t_0 (or τ, if $\tau > t_0$), but also for the bubston cluster coalescence; i.e., this intensity coincides with the threshold for inducing a stimulated optical coalescence (SOC) effect. We assume that $\tau >> t_0$. Thus, it is necessary to account for the effect of a laser pulse with an intensity $I = I_{thr}$ on the bubston expansion at $t > t_0$. The expansion process is considered to be quasi-static in the sense that definite electron temperature $T_e = T_e(R)$ corresponds to the moments of time $t > t_0$, and, accordingly, to each particular value of the bubble radius $R = R(t)$ for $R > R_0$. In this case the electron distribution $n_e(R)$ inside a bubston is governed by equation (A7) with the parameters R and $T_e(R)$. This means that there exists a maximum (limiting) average density of electrons $\langle n_e \rangle_{\max}(R) = (16/3)T_e^2(R)/(\pi e^4 R)$ and, accordingly, a maximum total number of electrons $N_{e\max}(R) = (64/9)T_e^2(R)R^2/e^4$ for each value of $R = R(t)$. The value of $N_{e\max}(R)$ at $R > R_0$ can either increase or decrease depending on the temperature $T_e(R)$.

The effect of pump radiation on bubston expansion means that in the process of growing the radius R new electrons can be generated due to the ionization of the bubston wall. It is clear that the number of electrons inside a bubston depends on the radius of bubston R and should be limited by the condition $N_e(R) < N_{e\max}(R)$. In this situation, the self-consistent expansion regime may set in, when the generation of new electrons is balanced by their losses due to adhesion to the wall. The dependence of T_e on R in the form $T_e(R) = T_e(R_0) \times (R_0/R)$, where $T_e(R_0) = \Delta/3$, fits this case. Intuition suggests that $N_{e\max}(R)$, which stands for the number of electrons under self-consistent conditions, should be close to its initial value $N_{e\max}(R_0) = 2 \times 10^5$, i.e., $N_e(R) \approx N_{e\max}(R_0) = 2 \times 10^5$. Indeed, the steady growth of R is realized under the small deviations of the value $\delta = N_e(R) - N_{e\max}(R_0)$, which are always balanced: at $\delta < 0$ these are balanced by the ionization of the wall, and at $\delta > 0$ these are compensated due to the adhesion of the electrons. At $\delta = 0$, these two processes are balanced by one another. This self-consistent expansion regime can actually be realized only for a certain range of R. We assume this regime is realized in the range $R_0 < R < R_1$, where R_1 is the radius of bubstons in the cluster, at which the coalescence starts.

The dynamics of the bubble expansion at $R > R_0$ are described by Equation (A14), which for convenience should be rewritten in another form. Considering the bubston radius R as an independent variable, we obtain

$$R\frac{du^2}{dR} + 3u^2 = 2\frac{p_e}{\rho}, \tag{A25}$$

where $u = dR/dt$, and the pressure p_e is described by Equation (A17) when replacing R_0 with R. In the self-consistent regime $\langle n_e \rangle(R) = \langle n_e \rangle_{\max}(R_0/R)^3$ and $x = x(R_0) = 8.4$ (see Equation (A9)). Thus, rewriting Equation (A17), we arrive at

$$p_e(R) = \rho u_0^2(1 + 2\mu)(R_0/R)^4, \tag{A26}$$

where u_0 is determined by the relationship (A19). Thus, the solution to Equation (A25) has the form

$$u(R) = \sqrt{2(1+2\mu)}u_0(R_0/R)^{3/2}(1+\eta-R_0/R)^{1/2}, \quad \text{(A27)}$$

where $\eta = u^2(R_0)/\left[2(1+2\mu)u_0^2\right]$. The maximum velocity $u(R_0)$, according to Equation (A18), is $u(R_0) = (1+\mu)u_0^2\theta(I_{thr})/R_0$, and therefore, taking Equations (A19) and (A20) into account, we obtain $\eta \approx \zeta/2 < 1$. At a sufficiently large expansion of bubstons in the cluster, they merge together into one large bubble; that is, the coalescence is completed. As a quantitative criterion of completing the coalescence, we impose the condition that the maximum radius of the expansion is $R_1 = l/2$, where l is the distance between the centers of the bubstons in the cluster. According to [29], $l \approx 2a_i$, where $a_i = \sqrt{\varepsilon T/(8\pi e^2 n_{i0})}$ is the Debye screening radius in aqueous electrolyte solution, see., e.g., [50]; here, T is temperature, and ε is the dielectric constant. According to the results of our preliminary measurements, the pH value for the water samples is pH $\approx$ 5.5. Such a value of pH is due to the dissolution of CO_2 in water, followed by its hydrolysis and the formation of carbonic acid H_2CO_3. After estimating $n_{i0} = 3 \times 10^{15}$ cm^{-3}, we obtain $a_i = 2 \times 10^{-5}$ cm. Under these conditions (these can be regarded as typical ones), the criterion of the coalescence has the form: $R_1/R_0 = a_i/R_0 \approx 2$. As follows from Equation (A27), the time duration necessary for such expansion (we shall refer to it as the coalescence time t_{coal}) is equal to

$$t_{coal} = \int_{R_0}^{a_i} \frac{dr}{u(R)} = \frac{R_0/u_0}{\sqrt{2(1+2\mu)}} \int_1^{a_i/R_0} \frac{z^{3/2}dz}{\sqrt{1+\eta-1/z}}.$$

Since $0 < \eta < 1$, this integral does not diverge in the vicinity of $z = 1$. Assuming $\eta \approx 0.01$, this integral at $a_i/R_0 \approx 2$ is equal to 3.5. Thus, for the coalescence time we have an estimate $t_{coal} = 10^{-10}$ s $\approx t_0$; i.e., the stimulated optical coalescence (SOC) of a bubston cluster occurs at the stage of inertial retention. Thus, it follows from here that if the pulse duration $\tau > t_{coal}$ (it means that $\tau > t_0 = 0.1 \times 10^{-9}$ s) and its intensity $I > I_{thr} = 9.6 \times 10^6$ W/cm^2, such a pulse should result in the SOC effect. Since the walls of the macroscopic bubble formed as a result of SOC remain positively charged, the free electrons inside the bubble must stick to these walls; that is, the effective charge of such a bubble must be close to zero. However, due to the presence of anions adsorbed on the inner surface of the bubston cluster, the charge of a macroscopic bubble cannot be exactly equal to zero. It can be shown, see Ref. [29], that despite the presence of an adsorbed charge, such a macroscopic bubble will not be ion-stabilized; i.e., such a bubble will rapidly collapse according to the kinetics described in the work [44].

Summarizing, we can say that stimulated optical coalescence sets in at laser intensities of about 10^7 W/cm^2. If the intensity of laser radiation significantly exceeds this threshold value, and if the laser pulse has not yet finished by the time the coalescence process is completed, the electrons continue to swing by the electromagnetic wave and collide with heavy particles ("fragments" of the liquid walls of the bubston cluster). However, these collisions are no longer elastic, the electrons lose their energy in these collisions, which leads to the effect of bremsstrahlung and an optical breakdown flash. It is the presence of a flash of breakdown that is the main feature of breakdown in classical experimental works on this subject, see review [13]. We also note that if the intensity exceeds the threshold value significantly, a breakdown flash will occur due to the laser radiation energy accumulated inside the coalesced cluster, i.e., a breakdown flash can also be realized for pulses with a duration of $\tau < t_{coal} = 10^{-10}$ s, i.e., for picosecond and femtosecond pulses. However, if the intensity in the pulse corresponds to the threshold conditions, i.e., about 10^7 W/cm^2, all the energy in the pulse is spent solely on the coalescence process, i.e., there is no breakdown flash at such intensities.

References

1. Alhejaili, W.; El-Nasr, M.A.; Lotfy, K.; El-Bary, A. Laser short-pulse effect on magneto-photo-elasto-thermodiffusion waves of fractional heat equation for non-local excited semiconductor. *Opt. Quantum Electron.* **2022**, *54*, 833. [CrossRef]
2. Lotfy, K.; Hassan, W.; Gabr, M.E. Thermomagnetic effect with two temperature theory for photothermal process under hydrostatic initial stress. *Results Phys.* **2017**, *7*, 3918–3927. [CrossRef]
3. Lotfy, K.; Hassan, W.; El-Bary, A.A.; Kadry, M.A. Response of electromagnetic and Thomson effect of semiconductor medium due to laser pulses and thermal memories during photothermal excitation. *Results Phys.* **2020**, *16*, 102877. [CrossRef]
4. Khamis, A.K.; Lotfy, K.; El-Bary, A.A.; Mahdy, A.M.S.; Ahmed, M.H. Thermal-piezoelectric problem of a semiconductor medium during photo-thermal excitation. *Waves Random Complex Media* **2021**, *31*, 2499–2513. [CrossRef]
5. Vogel, A.; Venugopalan, V. Pulsed Laser Ablation of Soft Biological Tissues. In *Optical-Thermal Response of Laser-Irradiated Tissue*, 1st ed.; Welch, A.J., van Gemert, M.J.C., Eds.; Springer: New York, NY, USA, 2011; pp. 551–615.
6. Kaschke, M.; Donnerhacke, K.-H.; Rill, M.S. *Optical Devices in Ophthalmology and Optometry: Technology, Design Principles and Clinical Applications*, 1st ed.; Wiley-VCH Verlag GmbH & Co. KGaA: Weinheim, Germany, 2014.
7. Bhargava, R.; Kumar, P.; Phogat, H.; Chaudhary, K.P. Neodymium-yttrium aluminium garnet laser capsulotomy energy levels for posterior capsule opacification. *J. Ophthalmic Vis. Res.* **2015**, *10*, 37–42. [CrossRef] [PubMed]
8. Vogel, A.; Noack, J.; Hüttman, G.; Paltauf, G. Mechanisms of femtosecond laser nanosurgery of cells and tissues. *Appl. Phys. B* **2005**, *81*, 1015–1047. [CrossRef]
9. Vogel, A.; Busch, R.; Parlitz, U. Shock wave emission and cavitation bubble generation by picosecond and nanosecond optical breakdown in water. *J. Acoust. Soc. Am.* **1996**, *100*, 148–165. [CrossRef]
10. Latz, C.; Asshauer, T.; Rathjen, C.; Mirshahi, A. Femtosecond laser assisted surgery of the eye: Overview and impact of the low energy concept. *Micromachines* **2021**, *12*, 122. [CrossRef]
11. Tinne, N.; Knoop, G.; Kallweit, N.; Veith, S.; Bleeker, S.; Lubatschowski, H.; Krüger, A.; Ripken, T. Effects of cavitation bubble interaction with temporally separated fs-laser pulses. *J. Biomed. Opt.* **2014**, *19*, 048001. [CrossRef]
12. Lubatschowski, H.; Maatz, G.; Heisterkamp, A.; Hetzel, U.; Drommer, W.; Welling, H.; Ertmer, W. Application of ultrashort laser pulses for intrastromal refractive surgery. *Graefes Arch. Clin. Exp. Ophthalmol.* **2000**, *238*, 33–39. [CrossRef]
13. Kennedy, P.K.; Hammer, X.; Rockwell, B.A. Laser-induced breakdown in aqueous media. *Prog. Quantum Electron.* **1997**, *21*, 155–248. [CrossRef]
14. Bunkin, N.F.; Shkirin, A.V.; Ignatiev, P.S.; Chaikov, L.L.; Burkhanov, I.S.; Starosvetskiy, A.V. Nanobubble clusters of dissolved gas in aqueous solutions of electrolyte. I. Experimental proof. *J. Chem. Phys.* **2012**, *137*, 054706. [CrossRef]
15. Bunkin, N.F.; Shkirin, A.V. Nanobubble clusters of dissolved gas in aqueous solutions of electrolyte. II. Theoretical interpretation. *J. Chem. Phys.* **2012**, *137*, 054707. [CrossRef]
16. Nirmalkar, N.; Pacek, A.; Barigou, M. On the existence and stability of bulk nanobubbles. *Langmuir* **2018**, *34*, 10964–10973. [CrossRef]
17. Temesgen, T.; Bui, T.T.; Han, M.; Kim, T.I.; Park, H. Micro and nanobubble technologies as a new horizon for water-treatment techniques: A review. *Adv. Colloid Interface Sci.* **2017**, *246*, 40–51. [CrossRef]
18. Azevedo, A.; Oliveira, H.; Rubio, J. Bulk nanobubbles in the mineral and environmental areas: Updating research and applications. *Adv. Colloid Interface Sci.* **2019**, *271*, 101992. [CrossRef]
19. Svetovoy, V.B. Spontaneous chemical reactions between hydrogen and oxygen in nanobubbles. *Curr. Opin. Colloid Interface Sci.* **2021**, *52*, 101423. [CrossRef]
20. Yasuda, K.; Matsushima, H.; Asakura, Y. Generation and reduction of bulk nanobubbles by ultrasonic irradiation. *Chem. Eng. Sci.* **2019**, *195*, 455–461. [CrossRef]
21. Etchepare, R.; Oliveira, H.; Nicknig, M.; Azevedo, A.; Rubio, J. Nanobubbles: Generation using a multiphase pump, properties and features in flotation. *Miner. Eng.* **2017**, *112*, 19–26. [CrossRef]
22. Michailidi, E.D.; Bomis, G.; Varoutoglou, A.; Kyzas, G.Z.; Mitrikas, G.; Mitropoulos, A.C.; Efthimiadou, E.K.; Favvas, E.P. Bulk nanobubbles: Production and investigation of their formation/stability mechanism. *J. Colloid Interface Sci.* **2020**, *564*, 371–380. [CrossRef]
23. Ulatowski, K.; Sobieszuk, P.; Mróz, A.; Ciach, T. Stability of nanobubbles generated in water using porous membrane system. *Chem. Eng. Process.-Process Intensific.* **2019**, *136*, 62–71. [CrossRef]
24. Zhang, M.; Seddon, J.R. Nanobubble–nanoparticle interactions in bulk solutions. *Langmuir* **2016**, *32*, 11280–11286. [CrossRef] [PubMed]
25. Lee, J.I.; Huh, H.S.; Park, J.Y.; Han, J.G.; Kim, J.M. Coarsening behavior of bulk nanobubbles in water. *Sci. Rep.* **2021**, *11*, 19173.
26. Jadhav, A.J.; Barigou, M. On the clustering of bulk nanobubbles and their colloidal stability. *J. Col. Int. Sci.* **2021**, *601*, 816–824. [CrossRef] [PubMed]
27. Jadhav, A.J.; Barigou, M. Electrochemically Induced Bulk Nanobubbles. *Ind. Eng. Chem. Res.* **2021**, *60*, 17999–18006. [CrossRef]
28. Alheshibri, M.; Qian, J.; Jehannin, M.; Craig, V.S.J. A history of nanobubbles. *Langmuir* **2016**, *32*, 11086–11100. [CrossRef]
29. Bunkin, N.F.; Bunkin, F.V. Bubston structure of water and electrolyte aqueous solutions. *Phys.-Uspekhi* **2016**, *59*, 846–865. [CrossRef]
30. Bunkin, N.F.; Shkirin, A.V.; Suyazov, N.V.; Babenko, V.A.; Sychev, A.A.; Penkov, N.V.; Belosludtsev, K.N.; Gudkov, S.V. Formation and Dynamics of Ion—Stabilized Gas Nanobubble Phase in the Bulk of Aqueous NaCl Solutions. *J. Phys. Chem. B* **2016**, *120*, 1291. [CrossRef]

31. Yurchenko, S.O.; Shkirin, A.V.; Ninham, B.W.; Sychev, A.A.; Babenko, V.A.; Penkov, N.V.; Kryuchkov, N.P.; Bunkin, N.F. Ion-specific and thermal effects in the stabilization of the gas nanobubble phase in bulk aqueous electrolyte solutions. *Langmuir* **2016**, *32*, 11245–11255. [CrossRef]
32. Bunkin, N.F.; Suyazov, N.V.; Shkirin, A.V.; Ignatiev, P.S.; Indukaev, K.V. Nano-scale structure of dissolved air bubbles in water as studied by measuring the elements of the scattering matrix. *J. Chem. Phys.* **2009**, *130*, 134308. [CrossRef]
33. Bunkin, N.F.; Suyazov, N.V.; Shkirin, A.V.; Ignatiev, P.S.; Indukaev, K.V. Cluster structure of stable dissolved gas nanobubbles in highly purified water. *JETP* **2009**, *108*, 800–816. [CrossRef]
34. Bunkin, N.F.; Ninham, B.W.; Ignatiev, P.S.; Kozlov, V.A.; Shkirin, A.V.; Starosvetskij., A.V. Long-living nanobubbles of dissolved gas in aqueous solutions of salts and erythrocyte suspensions. *J. Biophoton.* **2011**, *4*, 150–164. [CrossRef]
35. Bunkin, N.F.; Shkirin, A.V.; Kozlov, V.A. Cluster Structure of Dissolved Gas Nanobubbles in Ionic Aqueous Solutions. *J. Chem. Eng. Data* **2012**, *57*, 2823–2831. [CrossRef]
36. Vanraes, P.; Bogaerts, A. Plasma physics of liquids–a focused review. *Appl. Phys. Rev.* **2018**, *5*, 031103. [CrossRef]
37. Babenko, V.A.; Bunkin, N.F.; Sychev, A.A.; Suyazov, N.V. Plasmon enhanced low frequency stimulated Raman scattering in water due to optical breakdown in gas nanobubbles. *J. Opt.* **2020**, *22*, 015401. [CrossRef]
38. Babenko, V.A.; Bunkin, N.F.; Sychev, A.A. Role of gas nanobubbles in nonlinear hyper-Raman scattering of light in water. *J. Opt. Soc. Am. B* **2020**, *37*, 2805–2814. [CrossRef]
39. Babenko, V.A.; Bunkin, N.F.; Sychev, A.A. Nonlinear light scattering spectra in water: Dependence on the content of dissolved gas and effects of non-stationarity. *J. Raman Spectrosc.* **2022**, *53*, 1070–1080.
40. Semak, V.V.; Gerakis, A.; Shneider, M.N. Measurement of temperature dependent absorption coefficient of water at 1064 nm wavelength. *AIP Adv.* **2019**, *9*, 085016. [CrossRef]
41. Van de Hulst, H.C. *Light Scattering by Small Particles*, 1st ed; John Wiley and Sons: New York, NY, USA, 1957.
42. Babenko, V.A.; Sychev, A.A. Ultrashort-pulse generation in a passive-mode-locked YAG:Nd laser by means of the resonator-loss-unloading method. *J. Russ. Laser Res.* **1999**, *20*, 478–487. [CrossRef]
43. Bazelyan, E.M.; Raizer, Y.P. *Spark Discharge*, 1st ed.; CRC Press: Boca Raton, NY, USA, 1997.
44. Ljunggren, S.; Eriksson, J.C. The lifetime of a colloid-sized gas bubble in water and the cause of the hydrophobic attraction. *Colloids Surf. A Physicochem. Eng. Asp.* **1997**, *129–130*, 151–155. [CrossRef]
45. Tanaka, M.; Girard, G.; Davis, R.; Peuto, A.; Bignell, N. Recommended table for the density of water between 0 °C and 40 °C based on recent experimental reports. *Metrologia* **2001**, *38*, 301–309. [CrossRef]
46. Bunkin, N.F.; Shkirin, A.V.; Penkov, N.V.; Goltayev, M.V.; Ignatiev, P.S.; Gudkov, S.V.; Izmailov, A.Y. Effect of Gas Type and Its Pressure on Nanobubble Generation. *Front. Chem.* **2021**, *9*, 630074. [CrossRef] [PubMed]
47. Thomas, R.J.; Hammer, D.X.; Noojin, G.D.; Stolarski, D.J.; Rockwell, B.A.; Roach, W.P. Time-resolved spectroscopy of laser induced breakdown in water. *Proc. SPIE* **1996**, *2681*, 402–410.
48. Nikogosyan, D.N.; Oraevsky, A.A.; Rupasov, V.I. Two-photon ionization and dissociation of liquid water by powerful laser UV radiation. *Chem. Phys.* **1983**, *77*, 131–143. [CrossRef]
49. Grand, D.; Bernas, A.; Amouyal, E. Photoionization of aqueous indole; conduction band edgeand energy gap in liquid water. *Chem. Phys.* **1979**, *44*, 73–79. [CrossRef]
50. Landau, L.D.; Lifshitz, E.M. *Statistical Physics, Course of Theoretical Physics, Vol. 5*, 2nd ed.; Pergamon Press: New York, NY, USA, 1969.
51. Ginzburg, V.L. *The Propagation of Electromagnetic Waves in Plasmas*, 2nd ed.; Pergamon Press: New York, NY, USA, 1970.
52. Lamb, H. *Hydrodynamics*, 6th ed.; Cambridge University Press: Cambridge, UK, 1994.

Disclaimer/Publisher's Note: The statements, opinions and data contained in all publications are solely those of the individual author(s) and contributor(s) and not of MDPI and/or the editor(s). MDPI and/or the editor(s) disclaim responsibility for any injury to people or property resulting from any ideas, methods, instructions or products referred to in the content.